Supporting information

Broadband emitting phosphor $Sr_6Sc_2Al_4O_{15}$:Cr^{3+} for near-infrared LEDs

Jinyi Wang, Xudong Wang, Chenjie Zhang, Xinyu Zhang, Tianliang Zhou[*] and Rong-Jun Xie[*]

Fujian Key Laboratory of Surface and Interface Engineering for High Performance Materials, College of Materials, Xiamen University, Xiamen 361005, P. R. China

Corresponding Authors

[*]E-mail: bible2@163.com (T.Z.).

[*]E-mail: rjxie@xmu.edu.cn (R.-J.X.).

Table S1. Excitation and emission peak wavelengths of some NIR phosphors.

Phosphor	λ_{ex} (nm)	λ_{em} (nm)	Spectral profile	Ref.
$MgGeO_3:Pr^{3+}$	254	625	Multi-narrowband	1
$K_3LuSi_2O_7:Eu^{2+}$	460	740	Broadband	2
$Sr_3Li_4Si_2N_6:Eu^{2+}$	450	800	Broadband	3
$Lu_3Sc_2Ga_3O_{12}:Yb^{3+}$	850	976	Multi-narrowband	4
$La_3Si_6N_{11}:Yb^{3+}$	365	983	Narrowband	5
$LaSrGaO_4:Nd^{3+}$	808	1076	Multi-narrowband	6
$Y_2Ti_2O_7:Bi^{3+}$	391	744	Broadband	7
$Cs_2ZnCl_4:Sb^{3+}$	316	745	Broadband	8
$FAPbI_3:Sn^{2+}$	510	784	Narrowband	9
$MgAl_2O_4:Mn^{4+}$	440	651	Broadband	10
$NaAlP_2O_7:Cr^{3+}$	450	790	Broadband	11
$MgAl_2O_4:Mn^{2+}$	450	825	Broadband	12
$CaMgGe_2O_6:Cr^{3+}$	450	845	Broadband	13
$CaMgSi_2O_6:Cr^{3+}$	455	845	Broadband	14
$LiGaP_2O_7:Cr^{3+}$	452	846	Broadband	15
$NaInP_2O_7:Cr^{3+}$	460	870	Broadband	16
$LiInGe_2O_6:Cr^{3+}$	460	880	Broadband	17
$Sr_2InSbO_6:Fe^{3+}$	340	885	Broadband	18
$NaScGe_2O_6:Cr^{3+}$	490	895	Broadband	19
$CaScAlSiO_6:Cr^{3+}$	460	950	Broadband	20
$ZnGa_2O_4:Ni^{2+}$	260	1240	Broadband	21

Table S2. Crystallographic data of SSA:xCr^{3+} (x = 0.008, 0.08).

Formula	SSA:$0.008Cr^{3+}$	SSA:$0.08Cr^{3+}$
Crystal system	monoclinic	monoclinic
Space group	C 2	C 2
a (Å)	17.2395	17.2370
b (Å)	5.6304	5.6293
c (Å)	7.5588	7.5549
α, β, γ (deg.)	90, 91.28, 90	90, 91.25, 90
Rwp (%)	3.62	3.72
Rp (%)	2.81	2.87
χ^2	1.64	1.76

Table S3. Atomic coordinates and isotropic displacement parameters of SSA.

Atom	x	y	z	Occupancy
Sc1	0.3448(6)	0.4815(3)	0.7557(3)	1
Sr1	0.1719(6)	0.4850(7)	0.5027(1)	1
Sr2	0.1626(5)	0.4695(6)	0.9714(5)	1

Atom	x	y	z	Occupancy
Sr3	0	0.0137(8)	0	0.5
Sr4	0	0.0610(4)	0.5	0.5
Al1	0.3115(7)	0.4793(8)	0.2457(6)	1
Al2	0.0165(3)	0.5065(5)	0.2249(5)	1

Table S4. Atomic coordinates and isotropic displacement parameters of SSA:$0.008Cr^{3+}$.

Atom	x	y	z	Occupancy
Sc1	0.3446(4)	0.5098(3)	0.7546(9)	0.996
Cr1	0.3446(4)	0.5098(3)	0.7546(9)	0.004
Sr1	0.1717(7)	0.5044(1)	0.5000(5)	1
Sr2	0.1618(4)	0.4866(2)	0.9704(5)	1
Sr3	0	0.0311(4)	0	0.5
Sr4	0	0.0871(1)	0.5	0.5
Al1	0.3112(6)	0.4862(2)	0.2434(9)	1
Al2	0.0153(4)	0.5350(9)	0.2273(7)	1

Table S5. Atomic coordinates and isotropic displacement parameters of SSA:$0.08Cr^{3+}$.

Atom	x	y	z	Occupancy
Sc1	0.3441(5)	0.5069(3)	0.7561(6)	0.96
Cr1	0.3441(5)	0.5069(3)	0.7561(6)	0.04
Sr1	0.1713(6)	0.5056(6)	0.5017(1)	1
Sr2	0.1624(4)	0.4904(8)	0.9709(2)	1
Sr3	0	0.0329(8)	0	0.5
Sr4	0	0.0857(9)	0.5	0.5
Al1	0.3114(5)	0.4879(1)	0.2422(7)	1
Al2	0.0164(1)	0.5370(5)	0.2299(5)	1

Table S6. ESR resonance signals of some Cr^{3+}-doped NIR phosphors.

Phosphors	Resonance signals		Ref.
	Isolated Cr^{3+} ions	Cr^{3+}-Cr^{3+} pairs	
$LiScGeO_4$	$g = 4.22$	$g = 1.97$	22
$Gd_{2.4}Lu_{0.6}Ga_4AlO_{12}$	$g = 4.22$	$g = 1.97$	23
Ga_4GeO_8	$g = 4.89$	$g = 2.02$	24
La_2MgHfO_6	/	$g = 1.99$	25
La_2MgZrO_6	$g = 4.22$	$g = 1.97$	26
$GdAl_3(BO_3)_4$	/	$g = 1.98$	27
$La_3Ga_{5.5}Nb_{0.5}O_{14}$	$g = 3.80$	$g = 1.94$	28
$LiScGeO_4$	$g = 3.878$	$g = 2.007$	29
$Lu_2CaMg_2Si_3O_{12}$	$g = 4.32$	$g = 1.98$	30

Table S6 lists the g value of some Cr doped NIR phosphors. The average g value was calculated

to be 4.22 ($\sigma^2 = 0.11$) and 1.98 ($\sigma^2 = 4.81*10^{-4}$) (representing the isolated Cr^{3+} ions and Cr^{3+}-Cr^{3+} pairs, respectively). Apparently, the *g* values of SSA:0.008Cr^{3+} are close to the average calculated *g* values.

Table S7. Binding energy of Cr^{3+} of some NIR phosphors.

Phosphors	Binding energy (eV)	Ref.
SnO_2	Cr-2p$_{1/2}$ (586.7); Cr-2p$_{3/2}$ (577.0)	31
$Sr_2P_2O_7$	Cr-2p$_{3/2}$ (577.0)	32
La_2MgHfO_6	Cr-2p$_{1/2}$ (586.3); Cr-2p$_{3/2}$ (576.3)	25
$K_2Ga_2Sn_6O_{16}$	Cr-2p$_{3/2}$ (576.01)	33
$Mg_7Ga_2GeO_{12}$	Cr-2p$_{1/2}$ (582.5)	34
$CaLu_2Mg_2Si_3O_{12}$	Cr-2p$_{3/2}$ (577.0)	35
Ga_4GeO_8	Cr-2p$_{3/2}$ (576.0)	24
$Gd_{2.4}Lu_{0.6}Ga_4AlO_{12}$	Cr-2p$_{3/2}$ (576.4; 580.9)	23
$LiScGeO_4$	Cr-2p$_{1/2}$ (586.7)	22

Table S7 lists the binding energy of Cr^{3+} of some NIR phosphors. The average binding energy of Cr^{3+} was calculated to be 576.53 eV ($\sigma^2 = 0.1834$) (representing the Cr-2p$_{3/2}$). Apparently, the binding energy of Cr^{3+} in SSA:0.008Cr^{3+} is close to the average value.

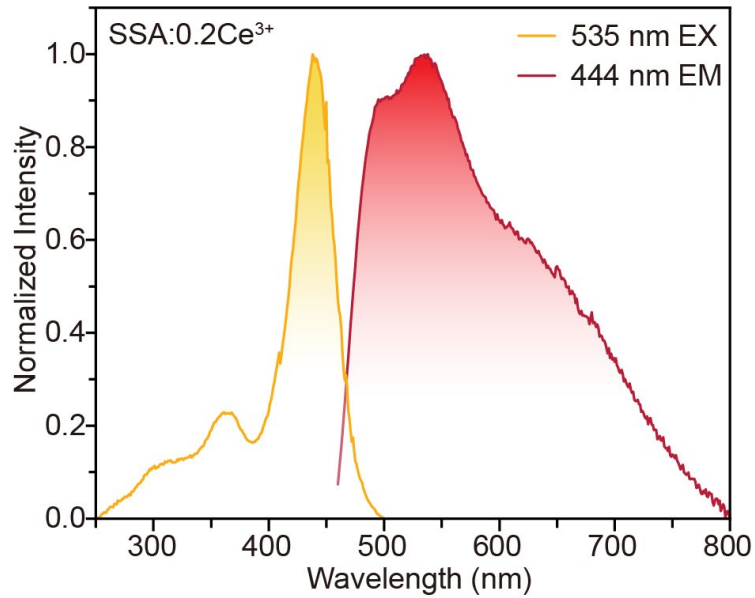**Fig. S1.** Photoluminescence and photoluminescence excitation spectra of SSA:0.2Ce^{3+}.
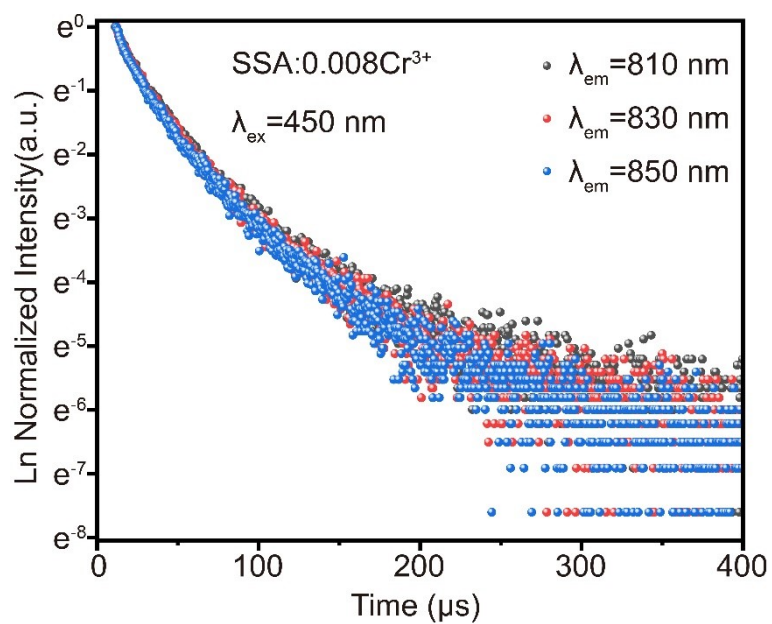
Fig. S2. Decay curves of SSA:0.008Cr^{3+} monitored at different wavelengths (810 nm, 830 nm and 850 nm, respectively).
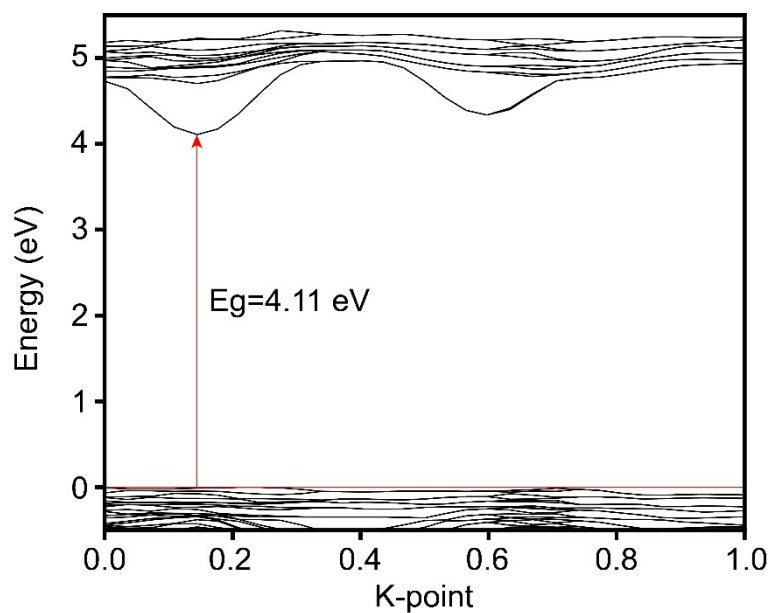

Fig. S3. Calculated band structure of $Sr_6Sc_2Al_4O_{15}$.

The calculation was performed via the density functional theory with the generalized gradient-corrected Perdew−Burke−Ernzerhof function. The kinetic energy cutoff and SCF tolerance were 340 eV and 10^{-5} eV/atom.
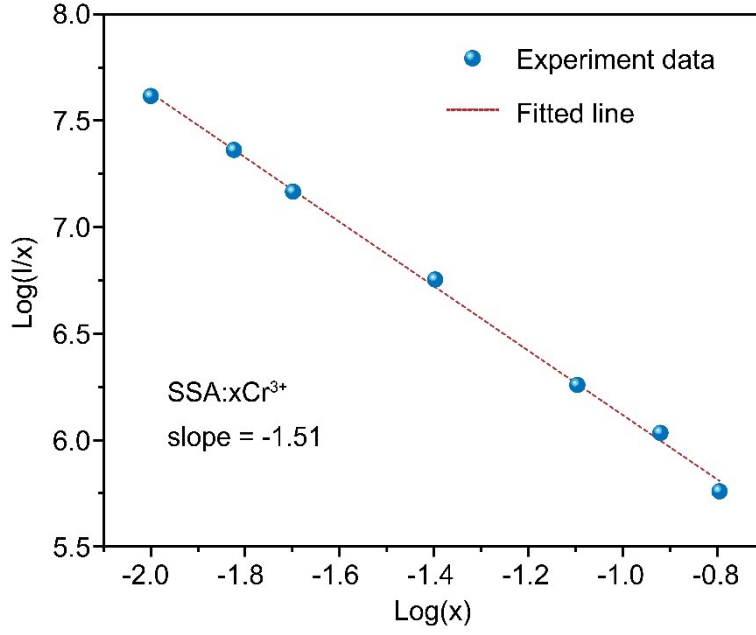
Fig. S4. Relationship between $\log(I/x)$ and $\log(x)$ of SSA:xCr^{3+} (x = 0-0.2).

Discussion:

The energy transfer and concentration quenching mechanism of phosphors are generally divided into three forms: exchange interaction, radiation recombination and electric multipolar interaction, which can be confirmed by calculating the R_c (the critical distance between adjacent Cr^{3+} ions) from the following formula:[36, 37]

$$R_c = 2\left(\frac{3V}{4\pi X_c N}\right)^{\frac{1}{3}} \tag{1}$$

Where V is the unite cell volume, N is the number of cations which can be occupied by Cr^{3+} in each unite cell, and X_c represents the doped concentration of Cr^{3+} ions. For SSA:$0.008Cr^{3+}$, N = 15, V = 776.376921 Å, X_c = 0.004, after calculation, the R_c is 29.13 Å, far greater than the maximum distance of exchange interaction (5 Å). So the energy transfer mechanism between Cr^{3+} should be the multipolar interaction. In addition, the large R_c of 29.13 Å illustrates that fewer Cr^{3+} ions can be accommodated in the limited crystal cell space, leading to a low quenching concentration. And according to the theory of Dexter, the type of interaction can be determined by the following equation:

$$\frac{I}{x} = \frac{k}{1 + \beta(x)^{\frac{\theta}{3}}} \tag{2}$$

Where I is the emission intensity, x is the concentration of Cr^{3+} beyond the optimal doping

concentration, k and β are the constants of the same excitation conditions. θ represents the characteristic number of electric multipolarity. θ = 6, 8 and 10 represents the dipole-dipole (d-d), dipole-quadrupole (d-q), and quadrupole-quadrupole (q-q) interactions, respectively. In order to obtain the value of θ, log(I/x) is plotted on the ordinate and log(x) is plotted on the abscissa, -θ/3 is the slope of the linearly fitting line. Fig. S4 shows that the value of -θ/3 is -1.51, so the value of θ is 4.53 (close to 6), which indicates that the quenching mechanism of Cr^{3+} is dipole-dipole (d-d) interaction in the SSA matrix.
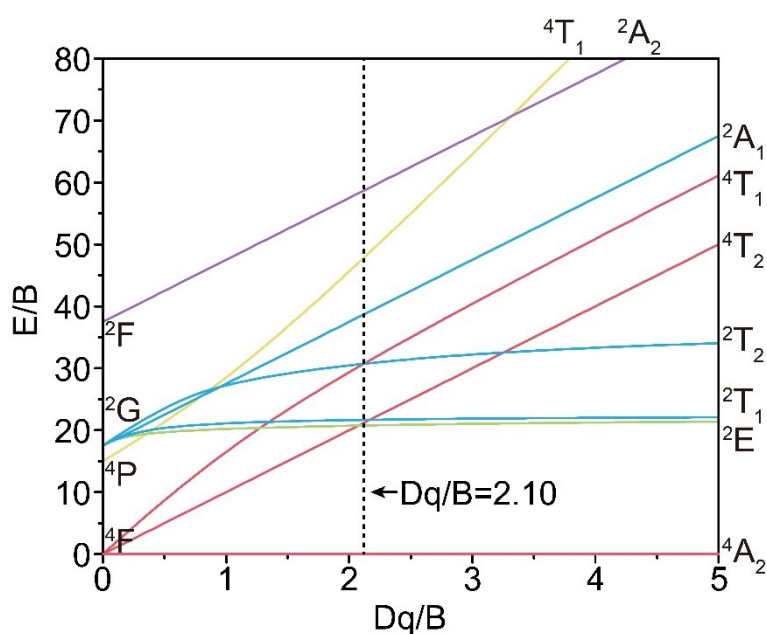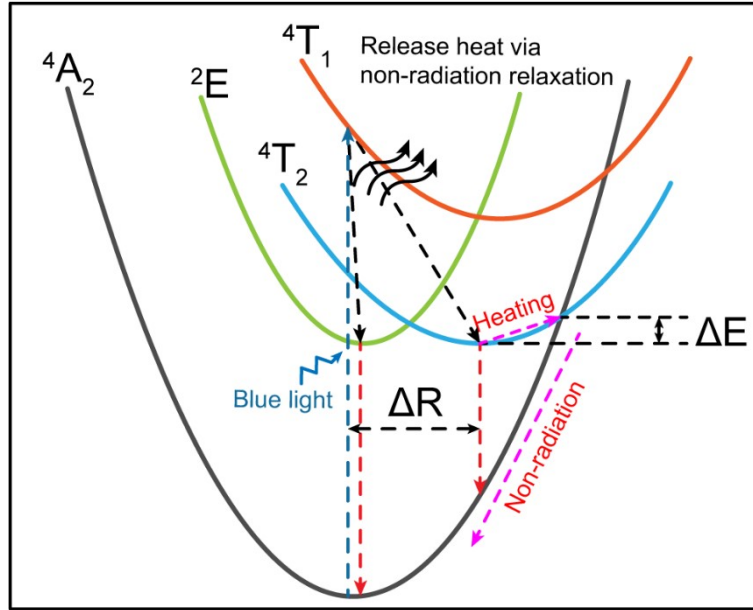

Fig. S5. Tanabe-Sugano diagram for the d^3 electronic configuration in an octahedral symmetry

For better understanding the interelectronic transitions that occur in d-orbitals, the Tanabe-Sugano diagram is illustrated in Fig. S5. According to the Tanabe–Sugano diagram, the relative energy position between the $^4T_2$ excited state and the $^4A_2$ ground state is strongly influenced by the crystal field strength (Dq/B). When Cr^{3+} is in an intermediate crystal field (Dq/B ~ 2.3), both $^2E{\rightarrow}^4A_2$ and $^4T_2{\rightarrow}^4A_2$ transitions can be observed in the emission spectra.[38] The value Dq/B of SSA:$0.008Cr^{3+}$, monitored at 860 nm, is calculated to be 2.10, belonging to the intermediate crystal field.

Configurational coordinate diagram

Fig. S6. The schematic configuration coordinate diagram of SSA:0.008Cr^{3+} in an intermediate crystal field

For the intermediate crystal field, the ^{2}E and ^{4}T$_2$ states are leveled to one another. When Cr^{3+} ions were excited by the blue light, the electrons in the ^{4}A$_2$ ground states transition to the ^{4}T$_1$ excited states and relax afterward into the lowest excited state ^{2}E and ^{4}T$_2$ via non-radiative relaxation, then returning to the ground state through ^{2}E→^{4}A$_2$ and ^{4}T$_2$→^{4}A$_2$ transitions. When the temperature is rising, the electrons in the excited state ^{4}T$_2$ will be excited to the intersection of ^{4}T$_2$ and ^{4}A$_2$ energy level, where the required energy ΔE is called activation energy. Then the electrons return to the ground state via non-radiative relaxation. The thermal stability depends on the offset (ΔR) between the two parabolas of the ground state and the lowest excited state, which is generally associated with the structural rigidity of host lattice.[39]
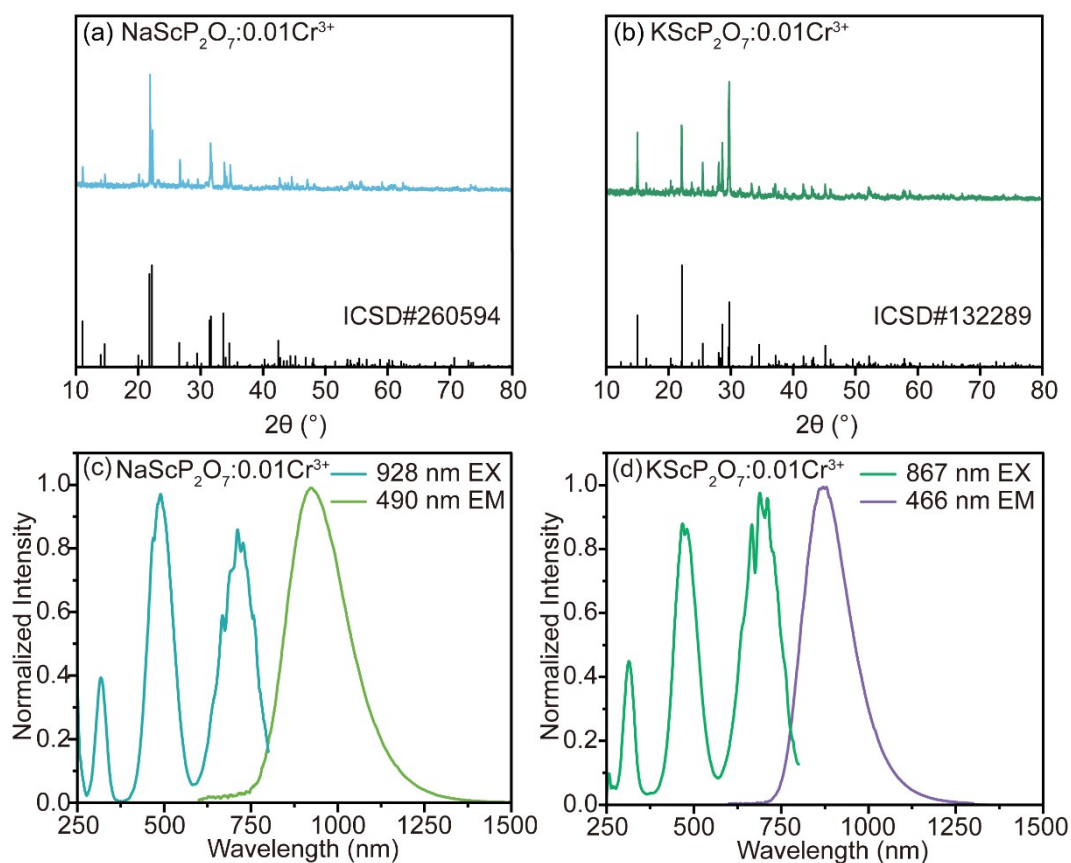
Fig. S7. XRD of (a) NaScP$_2$O$_7$:0.01Cr^{3+}; (b) KScP$_2$O$_7$:0.01Cr^{3+}. Photoluminescence and photoluminescence excitation spectra of (c) NaScP$_2$O$_7$:0.01Cr^{3+}; (d) KScP$_2$O$_7$:0.01Cr^{3+}.

NaScP$_2$O$_7$:0.01Cr^{3+} and KScP$_2$O$_7$:0.01Cr^{3+} were synthesized via the conventional high-temperature solid-state reactions using chemical reagents of Na$_2$CO$_3$ (AR, Xi Long Scientific, Shantou, China), K$_2$CO$_3$ (AR, Sinopharm Chemical Reagent, Shanghai, China), Sc$_2$O$_3$ (4N, ZhongNuo Advanced Material Technology, Beijing, China), NH$_4$H$_2$PO$_4$ (AR, Sinopharm Chemical Reagent, Shanghai, China) and Cr$_2$O$_3$ (4N, Xi Long Scientific, Shantou, China) as starting materials. The starting materials were finely mixed with alcohol in an agate mortar for 25 mins. Then, the mixtures were loaded into alumina crucibles and fired in a tube furnace at 573 K for 2 h, and then at 1273 K for 6 h under the reducing atmosphere (N$_2$: H$_2$ = 9:1 in volume). As shown in Fig. S7 (a-b), all of the NaScP$_2$O$_7$:0.01Cr^{3+} and KScP$_2$O$_7$:0.01Cr^{3+} peaks match well with the standard ICSD cards (ICSD#260594 and ICSD#132289), and no other impurities are detected, indicating that Cr^{3+} doping does not change the structure of the NaScP$_2$O$_7$ and KScP$_2$O$_7$ host. Moreover, as seen in Fig. S7 (c-d), NaScP$_2$O$_7$:0.01Cr^{3+} and KScP$_2$O$_7$:0.01Cr^{3+} show emission peaks of 928 and 867 nm as well as FWHM of 203 and 160 nm, respectively.

Reference

1. Y. Liang, F. Liu, Y. Chen, X. Wang, K. Sun and Z. Pan, *Dalton Trans.*, 2017, **46**, 11149-11153.
2. J. Qiao, G. Zhou, Y. Zhou, Q. Zhang and Z. Xia, *Nat. Commun.*, 2019, **10**, 5267-5273.
3. S. Li, M. Amachraa, C. Chen, L. Wang, Z. Wang, S. P. Ong and R.-J. Xie, *Matter*, 2022, **5**, 1924-1936.
4. P. R., V. P., S. V. Sravani, V. V., M. I.R., L. V. and J. C.K., *Mater. Res. Bull.*, 2018, **101**, 347-352.
5. S. Zhang, Z. Song, F. Zhao, S. Liu, H. Cai, S. Wang and Q. Liu, *J. Rare Earths*, 2021, **39**, 1484-1491.
6. Z. Xing, P. Li, S. Wu, C. Liu, D. Dai, X. Li, L. Zhang, D. Wang, Z. Yang and Z. Wang, *J. Lumin.*, 2020, **225**, 117352-117364.
7. X. Wang, F. Jahanbazi, J. Wei, C. U. Segre, W. Chen and Y. Mao, *ACS Appl. Mater. Interfaces*, 2022, **14**, 36834-36844.
8. B. Su, M. Li, E. Song and Z. Xia, *Adv. Funct. Mater.*, 2021, **31**, 2105316-2105325.
9. R. Begum, X. Y. Chin, M. Li, B. Damodaran, T. C. Sum, S. Mhaisalkar and N. Mathews, *Chem. Commun.*, 2019, **55**, 5451-5454.
10. H. Ji, X. Hou, M. S. Molokeev, J. Ueda, S. Tanabe, M. G. Brik, Z. Zhang, Y. Wang and D. Chen, *Dalton Trans.*, 2020, **49**, 5711-5721.
11. H. Zhang, J. Zhong, C. Li, L. Wang and W. Zhao, *J. Lumin.*, 2022, **251**, 119211-119218.
12. E. Song, X. Jiang, Y. Zhou, Z. Lin, S. Ye, Z. Xia and Q. Zhang, *Adv. Opt. Mater.*, 2019, **7**, 1901105-1901113.
13. L. Fang, L. Zhang, H. Wu, H. Wu, G. Pan, Z. Hao, F. Liu and J. Zhang, *Inorg. Chem.*, 2022, **61**, 8815-8822.
14. L. Fang, Z. Hao, L. Zhang, H. Wu, H. Wu, G. Pan and J. Zhang, *Mater. Res. Bull.*, 2022, **149**, 111725-111731.
15. C. Yuan, R. Li, Y. Liu, L. Zhang, J. Zhang, G. Leniec, P. Sun, Z. Liu, Z. Luo, R. Dong and J. Jiang, *Laser Photonics Rev.*, 2021, **15**, 2100227-2100234.
16. L. Zeng, J. Zhong, C. Li, Z. Zhuang, L. Chen and W. Zhao, *J. Lumin.*, 2022, **247**, 118909-118915.
17. T. Liu, H. Cai, N. Mao, Z. Song and Q. Liu, *J. Am. Ceram. Soc.*, 2021, **104**, 4577-4584.
18. D. Liu, G. Li, P. Dang, Q. Zhang, Y. Wei, L. Qiu, M. S. Molokeev, H. Lian, M. Shang and J. Lin, *Light: Sci. Appl.*, 2022, **11**, 112-121.
19. X. Zhou, W. Geng, J. Li, Y. Wang, J. Ding and Y. Wang, *Adv. Opt. Mater.*, 2020, **8**, 1902003-1902010.
20. G. Liu, M. S. Molokeev and Z. Xia, *Chem. Mater.*, 2022, **34**, 1376-1384.
21. T. Liu, Z. Liu, J. Wu, K. Zhang, H. An, Z. Hu, S. Deng, X. Li and H. Li, *New J. Chem.*, 2022, **46**, 851-856.
22. Z. Ye, Z. Wang, Q. Wu, X. Huo, H. Yang, Y. Wang, D. Wang, J. Zhao, H. Suo and P. Li, *Dalton Trans.*, 2021, **50**, 10092-10101.
23. X. Zou, X. Wang, H. Zhang, Y. Kang, X. Yang, X. Zhang, M. S. Molokeev and B. Lei, *Chem. Eng. J.*, 2022, **428**, 132003-132011.
24. L. Yao, Q. Shao, M. Shi, T. Shang, Y. Dong, C. Liang, J. He and J. Jiang, *Adv. Opt. Mater.*, 2022, **10**, 2102229-2102238.
25. H. Suo, Y. Wang, X. Zhao, X. Zhang, L. Li, K. Guan, W. Ding, P. Li, Z. Wang and F. Wang, *Laser Photonics Rev.*, 2022, **16**, 2200012-2200019.
26. H. Zeng, T. Zhou, L. Wang and R.-J. Xie, *Chem. Mater.*, 2019, **31**, 5245-5253.

27. D. Huang, H. Zhu, Z. Deng, H. Yang, J. Hu, S. Liang, D. Chen, E. Ma and W. Guo, *J. Mater. Chem. C*, 2021, **9**, 164-172.

28. Y. Li, S. Ye and Q. Zhang, *J. Mater. Chem. C*, 2014, **2**, 4636-4641.

29. S. Miao, Y. Liang, Y. Zhang, D. Chen and X. Wang, *ACS Appl. Mater. Interfaces*, 2021, **13**, 36011-36019.

30. W. Nie, L. Yao, G. Chen, S. Wu, Z. Liao, L. Han and X. Ye, *Dalton Trans.*, 2021, **50**, 8446-8456.

31. J. C. R. Aquino, F. H. Aragón, J. A. H. Coaquira, X. Gratens, V. A. Chitta, I. Gonzales, W. A. A. Macedo and P. C. Morais, *J. Phys. Chem. C*, 2017, **121**, 21670-21677.

32. S. Jiao, R. Pang, S. Wang, H. Wu, T. Tan, S. Zhang, L. Jiang, D. Li, C. Li and H. Zhang, *Mater. Res. Bull.*, 2022, **149**, 111710-111717.

33. J. a. Lai, W. Shen, J. Qiu, D. Zhou, Z. Long, Y. Yang, K. Zhang, I. Khan and Q. Wang, *J. Am. Ceram. Soc.*, 2020, **103**, 5067-5075.

34. G. Wei, P. Li, R. Li, J. Li, Y. Shi, Y. Wang, S. He, Y. Yang, H. Suo and Z. Wang, *Inorg. Chem.*, 2022, **61**, 5665-5671.

35. R. Li, Y. Liu, C. Yuan, G. Leniec, L. Miao, P. Sun, Z. Liu, Z. Luo, R. Dong and J. Jiang, *Adv. Opt. Mater.*, 2021, **9**, 2100388-2100394.

36. C. Tao, Z. Wang, Z. Li, N. Zhang, Z. Yang and P. Li, *J. Alloys Compd.*, 2019, **788**, 1000-1008.

37. G. Blasse, *Phys. Lett. A*, 1968, **28**, 444-445.

38. G. N. A. De Guzman, M. Fang, C. Liang, Z. Bao, S. Hu and R. Liu, *J. Lumin.*, 2020, **219**, 116944-116952.

39. T. Gao, R. Liu, Y. Liu, X. Chen and X. Ma, *J. Lumin.*, 2022, **246**, 118799.